

ARTICLE

Vibrational Spectra and Density Functional Theory Calculations of Metallo-tetra-(*tert*-butyl)-tetra-azaporphyrines

Tong-tong Lu, Hui-ling Gao, Tian-jing He, Fan-chen Liu, Dong-ming Chen*

Department of Chemical Physics, University of Science and Technology of China, Hefei 230026, China

(Dated: Received on April 30, 2010; Accepted on June 3, 2010)

The infrared absorption and 514.5 nm excited Raman spectra were measured for the metallo-tetra-(*tert*-butyl)-tetraazaporphyrin (MT(*t*Bu)TAP, M=Cu, Co, Ni, Zn). The ground-state structures and vibrational spectra of MT(*t*Bu)TAPs have been calculated at the B3LYP level of theory. The observed Raman and IR bands have been assigned based on the calculation results and by comparing with the normal metalloporphyrins. The relationship between the Raman/IR frequencies and the structures of TAP ring was investigated. The results show that the frequencies of $C_{\beta}C_{\beta}'$ stretch (A_g), asymmetric $C_{\alpha}N_m$ stretch (A_g), and symmetric $C_{\alpha}N_m$ stretch (B_g) modes increase linearly with the decrease of the core-sizes of TAP ring. Among the three modes, the later two are more sensitive to the core-size change.

Key words: Tetraazaporphyrin, Raman spectrum, Molecular vibration, Density functional theory

I. INTRODUCTION

Tetraazaporphyrin (TAP), also known as porphyrazine (Pz), is formed by bridging four pyrrole rings via four aza nitrogen atoms. They are structural intermediates connecting normal porphyrins (Pors) and phthalocyanines (Pcs). TAPs are applied to diverse areas such as biomedical agents for diagnosis and therapy, precursors to new conducting materials, chemical sensors, ladder polymers, and dyes [1–6]. As they share structural similarities with the porphyrins and the phthalocyanines, the spectroscopic studies of TAPs are expected to lead to a better understanding of the structures and properties of normal porphyrins and phthalocyanines.

On the other hand, tetraazaporphyrins show several unique and interesting properties distinct from phthalocyanines and porphyrins, which makes them the subject of increasing interest in their synthesis, properties, and applications [7–9]. In recent years, various substituted tetraazaporphyrins have been prepared via new synthetic routes or by using new starting materials, making them more accessible for spectroscopic studies [3, 4]. Kobayashi *et al.* reported the synthesis and electronic absorption spectrum of CoT(*t*Bu)TAP as a part of a series of cobaltic compounds with different molecular sizes [10]. They also reported the IR spectra and quantum-mechanical calculations of free-base, cobalt and copper tetraazaporphyrins (TAPs) [11]. Chen *et al.*

studied the optical absorption spectra of several metalotetraazaporphyrins, showing the influences of different central metal ions on the Q band absorption [12, 13]. Freyer *et al.* studied the absorption, luminescence, and Raman spectroscopic properties of a set of metal-free benzo-annelated tetraazaporphyrin films [14]. Strong bathochromic shift of Q-band absorption was found for increasing annelated benzo-moiety. A single broad featureless luminescence band with a large Stokes shift was observed for the films, which was thought originating from excitonic coupling [14]. Theoretical computations using density functional theory (DFT) were carried out for several TAPs and MTAPs to explore their atomic scale structures, mechanism of charge transport, and optical properties [15, 16].

Raman and IR spectra play an important role in the structural and dynamic studies of porphyrin-related compounds, including the Pcs and TAPs [17–22]. Theoretically, DFT calculations have been used to study the vibrational spectra of porphyrin-related compounds in recent years [11, 21–26]. It has been proven that current density functionals are capable of predicting the infrared and Raman spectra not only in the band positions but also in the intensities. While Kobayashi *et al.* have reported IR properties of free-base, cobalt and copper tetraazaporphyrins and interpreted some of the characteristic IR bands on the basis of the DFT calculations [11], detailed descriptions of vibrational modes of TAPs are still not well understood. In this work, we studied IR and Raman spectroscopic properties of MT(*t*Bu)TAP (M=Co, Ni, Cu, and Zn) together with density functional theory calculations in order to obtain more detailed knowledge about the vibrational states of these complexes.

* Author to whom correspondence should be addressed. E-mail: dmchen@ustc.edu.cn, Tel.: +86-551-3606145

II. EXPERIMENTAL AND COMPUTATIONAL METHODS

The analytic grade free-base tetra-(*tert*-butyl)-tetraazaporphyrin ($H_2T(tBu)TAP$) was purchased from Aldrich and used as received. The metal complexes, $MT(tBu)TAP$ ($M=Cu, Ni, Co, Zn$), were synthesized according to the traditional route for metal-chelation of the porphyrin compounds, *i.e.*, by treating the metal-acetate and free base $H_2T(tBu)TAP$ in hot dimethyl formamide (DMF) [11]. For copper complex ($CuT(tBu)TAP$), the synthesis details are as follows. Reagent-grade DMF (20 mL) was brought gently to a reflux on a hot plate and magnetically stirred to 50 °C. The solid $H_2T(tBu)TAP$ (10 mg) was added into the solvent and allowed to dissolve completely for a few minutes. Then 0.063 g copper acetate ($Cu(CH_3COO)_2 \cdot 2H_2O$) was added into the solution. Reaction was allowed to proceed for about 15 min. Complete conversion to the copper complex was checked by the UV-visible absorption spectrum, in which the four Q-bands of $H_2T(tBu)TAP$ were replaced by two Q-bands of $CuT(tBu)TAP$. After the reaction mixture cooled, equal volume of distilled water was added into the reaction mixture to precipitate the $CuT(tBu)TAP$ species. The product was separated with a centrifuge and washed with water to remove unreacted copper acetate, until the solution is clear. The obtained solid sample was then silica-gel dried in a desiccator. Similar procedures were used for preparing the cobalt, nickel, and zinc complexes.

IR spectra of $MT(tBu)TAP$ solid powders were measured on a Nicolet MAGNA-IR750 infrared spectrometer as KBr pellets. Solid Raman spectra were measured on a Labram-010 micro-Raman spectrometer. The 514.5 nm line of an Ar^+ laser (Spectra-Physics 163-C12) was used as the excitation source with the power of 5 mW on samples. The time constant of the air-cooled CCD detector was 20 s, and 4 scans were accumulated for each Raman spectrum.

DFT calculations for the ground state optimizations and IR/Raman spectra of $MT(tBu)TAP$ were carried out using the Becke's three-parameter hybrid functional (referred as B3LYP) [27, 28]. Standard 6-31G(d) basis sets were used for C, N, and H; while Ahlrichs' TZVP basis sets for Co, Ni, Cu, and Zn [29, 30]. The stability of the optimized geometries was confirmed by frequency calculations, which gave positive values for all the obtained frequencies. Assignment of individual vibrational frequency was carried out by inspecting the calculated Cartesian displacements of the corresponding mode. All calculations were performed with the Gaussian 03 [31] program suite on a P4-3.0G computer. As DFT-calculations are known to systematically overestimate harmonic frequencies, the resultant theoretical frequencies were scaled with a single factor of 0.97. The same factor has been used in the DFT calculations of porphyrin analogues by other researchers [32–34].

TABLE I B3LYP calculated bond lengths and bond angles of $CuT(tBu)TAP$, $CoT(tBu)TAP$, $NiT(tBu)TAP$, and $ZnT(tBu)TAP^a$.

	Cu	Co	Ni	Zn
Bond length/Å				
$C_\alpha C_\beta$	1.451	1.448	1.446	1.454
$C_\alpha' C_\beta'$	1.477	1.473	1.471	1.480
$C_\beta C_\beta'$	1.365	1.363	1.361	1.367
$C_\beta' C_1$	1.518	1.519	1.518	1.518
$C_\alpha N_m$	1.331	1.327	1.323	1.337
$C_\alpha' N_m$	1.330	1.326	1.323	1.336
$C_\alpha N_p$	1.368	1.372	1.372	1.367
$C_\alpha' N_p$	1.370	1.375	1.376	1.368
MN_p	1.951	1.919	1.902	1.984
Bond angle/(°)				
$C_\alpha N_p C_\alpha'$	107.5	106.3	105.8	108.4
$C_\alpha N_m C_\alpha'$	123.4	122.4	121.7	124.7
$C_\beta' C_\alpha' N_p$	109.8	110.5	110.8	109.2
$C_\beta C_\alpha N_p$	109.3	109.9	110.3	108.7
$C_\alpha' C_\beta' C_\beta$	105.2	105.1	105.0	105.4
$C_\alpha C_\beta C_\beta'$	108.3	108.2	108.1	108.4

^a With 6-31G(d) basis sets for C, N, H; TZVP for Cu, Co, Ni, Zn.

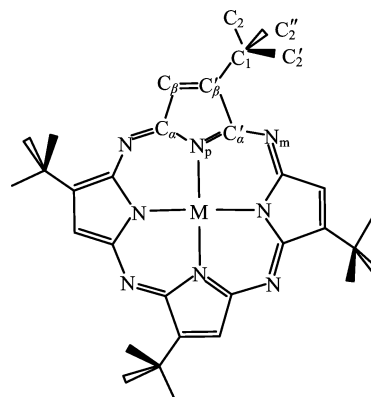


FIG. 1 Structural sketch of $MT(tBu)TAP$ showing the labels of the atoms.

III. RESULTS AND DISCUSSION

A. Ground state geometry

DFT geometry optimizations for $MT(tBu)TAP$ ($M=Co, Ni, Cu, Zn$) show that all the four complexes exhibit C_{4h} symmetry. The predicted bond lengths and bond angles are shown in Table I and the structure sketch with the atomic labels is displayed in Fig.1. Due to the *tert*-butyl substitution on the C_β' atoms, the pyrrole rings of $MT(tBu)TAP$ show dramatic in-plane deformation. For instance, the $C_\alpha' C_\beta'$ bonds are increased by 0.025–0.026 Å as compared with the $C_\alpha C_\beta$

bonds for the studied species. Also, the $C_\alpha N_p$ bonds are increased by 0.001–0.004 Å as compared with the $C_\alpha N_p$ bonds. The $C_\alpha C_\beta C_\beta'$ angles are larger than the $C_\alpha' C_\beta' C_\beta$ angles by $\sim 3^\circ$, whereas the $C_\beta' C_\alpha' N_p$ angles are larger than the $C_\beta C_\alpha N_p$ angles by $\sim 0.5^\circ$. This asymmetric deformation of the pyrrole rings is expected to have a significant effect on the vibrational states of MT(*t*Bu)TAPs.

As shown in Table I, the M– N_p bond-lengths were calculated to be 1.984, 1.951, 1.919, and 1.902 Å, respectively, for ZnT(*t*Bu)TAP, CuT(*t*Bu)TAP, CoT(*t*Bu)TAP, and NiT(*t*Bu)TAP. The general trend of M– N_p bond-length change is coincident with the order of the radius of central metal atoms: Zn>Cu>Co>Ni, reflecting that a larger metal atom requires a larger coordinating core to accommodate it.

The out-ring bonds of MT(*t*Bu)TAPs, $C_\beta C_\beta'$ and $C_\alpha N_m/C_\alpha' N_m$, show elongation in the order Zn>Cu>Co>Ni, manifesting an expansion of the out-ring with the increase of the metal size. Especially, the $C_\alpha N_m$ and $C_\alpha' N_m$ bond-lengths show large differences (0.014 and 0.013 Å, respectively) for different MT(*t*Bu)TAPs. The $C_\alpha N_m C_\alpha'$ bond angles also show evident changes, with ZnT(*t*Bu)TAP to be the largest (124.7°) and NiT(*t*Bu)TAP to be the smallest (121.7°). The large differences in the $C_\alpha N_m/C_\alpha' N_m$ bond-lengths and $C_\alpha N_m C_\alpha'$ bond-angles for different complexes indicate that the expansion/shrinkage of TAP ring is mainly via adapting the positions of meso-nitrogen atoms. On the other hand, the $C_\beta C_\beta'$ and $C_\alpha C_\beta/C_\alpha' C_\beta'$ bonds show only moderate changes (0.006 and 0.008/0.009 Å), reflecting that the pyrrole rings are less influenced by different metal chelations due to its rigidity.

B. Vibrational spectra

1. General consideration for the vibrations of MT(*t*Bu)TAP

MT(*t*Bu)TAP has 81 atoms and $3n-6=237$ degrees of internal freedom, which, according to the C_{4h} group, can be classified as:

$$\Gamma = 34A_g + 35B_g + 25A_u + 25B_u + 48E_g + 70E_u \quad (1)$$

For normal metalloporphyrins, a simplified planar D_{4h} molecular model, in which all peripheral substituents are represented by point masses, is often used in their vibrational analyses [19–21]. The molecular vibrations of a porphyrin compound can thus be divided into the porphyrin skeletal modes and the substituent internal modes, despite of the fact that the motions of the skeletal atoms and the substituent atoms are correlated with each other [19–21]. The vibrations of macrocycle ring can be further divided into the in-plane (ip) skeletal modes and the out-of-plane (oop) skeletal modes. By using this simplified model, the skeletal modes of

MT(*t*Bu)TAP can be classified as

$$\Gamma_{\text{TAP-ip}} = 15A_g + 16B_g + 16E_u \quad (2)$$

$$\Gamma_{\text{TAP-oop}} = 8A_u + 8B_u + 7E_g \quad (3)$$

The *tert*-butyl modes of MT(*t*Bu)TAP can be classified as:

$$\Gamma_{t\text{Bu}} = 19A_g + 19B_g + 17A_u + 17B_u + 17E_g + 19E_u \quad (4)$$

Among these vibrations, the A_u and E_u modes are IR active while the A_g , B_g , and E_g modes are Raman active [19–21, 35]. In the following sections, the IR/Raman bands of MT(*t*Bu)TAP will be assigned to local coordinates in which the phasing of adjacent bond stretches within the pyrrole rings and at the meso-nitrogen bridges are taken into account [19]. Since the calculated IR and Raman spectra of the four compounds are generally similar, our discussions will concentrate on CuT(*t*Bu)TAP.

2. Infrared spectra

Figure 2 shows the measured IR absorption spectra of MT(*t*Bu)TAP (M=Co, Ni, Cu, Zn) in KBr pellets. Figure 3 compares the experimental and theoretical IR spectra of CuT(*t*Bu)TAP, where the theoretical IR spectrum was simulated from the B3LYP calculated harmonic frequencies (scaled with 0.97) and intensities. By comparing with the DFT-calculated band positions and intensities, the observed IR bands of CuT(*t*Bu)TAP are assigned as listed in Table II. The mode numbers and the corresponding local coordinates in Table II (and also in Tables III and IV) follow those used in the vibrational study of normal metalloporphyrins [19, 21]. It is noticed that, while both A_u and E_u modes are IR active, B3LYP calculations indicate that most of the strong IR absorptions of CuT(*t*Bu)TAP in the high frequency region ($900-1600 \text{ cm}^{-1}$) belong to the E_u modes.

In the $1450-1650 \text{ cm}^{-1}$ region, the strong IR bands were measured at 1564, 1481, and 1460 cm^{-1} . The 1564 cm^{-1} band can be assigned to the $C_\beta C_\beta'$ stretching mode (ν_{38}), which was calculated at 1563 cm^{-1} with a considerable intensity. The absorption band observed at 1460 cm^{-1} is considered to be the scissoring vibration of the methyl group which was calculated at 1483 cm^{-1} . The IR band observed at 1481 cm^{-1} may be due to the overlap of the asymmetric $C_\alpha N_m$ stretching (ν_{37}) vibration (calculated at 1494 cm^{-1}) and the CH_3 scissoring (calculated at 1509 cm^{-1}), since in CoT(*t*Bu)TAP and NiT(*t*Bu)TAP we found two bands in nearby region. The IR bands observed at 1389 and 1360 cm^{-1} are probably due to the CH_3 umbrella vibrations, which were calculated at 1411 and 1382 cm^{-1} , respectively.

The strongest absorption in the region $1000-1300 \text{ cm}^{-1}$ was observed at 1011 cm^{-1} in the IR spectrum of CuT(*t*Bu)TAP, which is thought corresponding to the strongest 1007 cm^{-1} band by

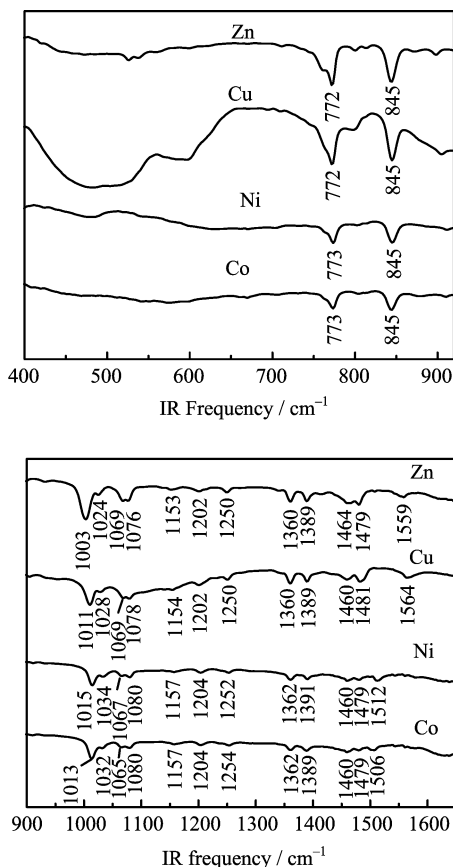


FIG. 2 Experimental infrared transmission spectra of MT(*t*Bu)TAP (M=Co, Ni, Cu, Zn; as KBr pellets).

calculation. This band is assigned to the pyrrole breathing vibration (ν_{47} , E_u symmetry). Two middle strong IR bands were observed at 1069 and 1078 cm^{-1} , whereas only a single strong absorption was calculated at 1066 cm^{-1} . According to the calculation, this band can be assigned to the asymmetric pyrrole half-ring stretch (ν_{44}). The DFT calculation also manifests that this mode is strongly mixed with the CH_3 wagging vibration, which may be responsible for its splitting in the experimental spectrum.

In 1000–1450 cm^{-1} region, additional weak absorption bands were observed at 1432, 1250, 1202, 1154, and 1028 cm^{-1} . Based on the B3LYP calculation, we assigned them to the symmetric $\text{C}_\alpha\text{N}_m$ stretching (ν_{39}), C_βH bending (ν_{51}), symmetric pyrrole half ring stretch (ν_{41}), C_βH bending (ν_{52}), and CH_3 wagging, respectively.

In the low frequency region (400–900 cm^{-1}), the measured IR bands at 799 and 772 cm^{-1} are considered corresponding to the calculated IR bands at 785 and 753 cm^{-1} . DFT calculation manifests that they are attributable to the asymmetric (ν_{46}) and symmetric pyrrole deformation (ν_{48}). The strong IR bands observed at 845 cm^{-1} (calculated at 844 cm^{-1}) is assigned to the out of plane bending of C_βH (γ_8), which is predicted

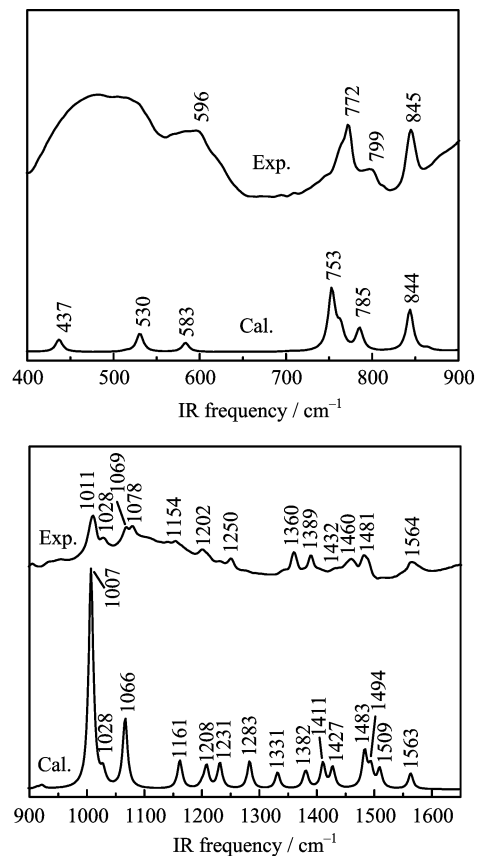


FIG. 3 Calculated and experimental (KBr pellet) infrared absorption spectra of CuT(*t*Bu)TAP.

by DFT calculation to be the sole strong band with A_u symmetry. The weak band observed at 596 cm^{-1} corresponds to the calculated IR band at 583 cm^{-1} . DFT calculation indicates that this mode involves the in-phase bending of $\text{C}_2\text{C}_1\text{C}'_2/\text{C}_2\text{C}_1\text{C}''_2/\text{C}'_2\text{C}_1\text{C}''_2$ angles and is actually the umbrella mode of $\text{C}(\text{CH}_3)_3$ group.

Our B3LYP calculation also predicted two IR bands at 530 and 437 cm^{-1} which can be assigned to the pyrrole rotation (ν_{49}) and $\text{Cu}-\text{N}_p$ stretching (ν_{50}) vibrations, respectively. They were not observed in our experiment because of the interference of very broad background in the low-frequency region.

C. Raman spectra

1. Raman spectra of CuT(*t*Bu)TAP

Figure 4 shows the 514.5 nm excited Raman spectrum of CuT(*t*Bu)TAP (solid powder) as well as DFT calculated Raman spectrum. Assignments of the skeletal vibrations of CuT(*t*Bu)TAP have been proposed with the help of DFT calculations and the results are listed in Table III (A_g modes) and Table IV (B_g modes).

The stretching vibrations of $\text{C}_\beta\text{C}_\beta'$ and $\text{C}_\alpha\text{N}_m/\text{C}_\alpha'\text{N}_m$ bonds are expected to appear in

TABLE II B3LYP-calculated and observed infrared frequencies (in cm^{-1}) of CuT(*t*Bu)TAP.

E _u modes			A _u modes		
Cal. ^a	Obs. ^b	Assign. ^c	Cal. ^a	Obs. ^b	Assign. ^c
1563	1564	$\nu_{38} \nu(\text{C}_\beta\text{C}_\beta')$	1492		CH ₃ scis.
1509		CH ₃ scis.	1479		CH ₃ scis.
1494	1481	$\nu_{37} \nu(\text{C}_\alpha\text{N}_m)_{\text{as}}$	1463		CH ₃ scis.
1483	1460	CH ₃ scis.	1379		CH ₃ umbr.
1477		CH ₃ scis.	1200		$\nu(\text{C}_1\text{C}_2')/\nu(\text{C}_1\text{C}_2'')$
1427	1432	$\nu_{39} \nu(\text{C}_\alpha\text{N}_m)_s$	1035		CH ₃ wag
1411	1389	CH ₃ umbr.	950		CH ₃ wag
1382	1360	CH ₃ umbr.	913		CH ₃ wag
1331		$\nu_{40} \nu(\text{Pyr}/4)$	844	845	$\gamma_8 \gamma(\text{C}_\beta\text{H})$
1283		$\nu_{43} \delta(\text{C}_\beta\text{H})/\nu(\text{C}_\beta'\text{C}_1)$	764		$\gamma_5(\text{Pyr fold})_s$
1231	1250	$\nu_{51} \delta(\text{C}_\beta\text{H})/\nu(\text{C}_\beta'\text{C}_1)$	704		$\gamma_1(\text{Pyr fold})_{\text{as}}$
1208	1202	$\nu_{41} \nu(\text{Pyr}/2)_s$	515		$\gamma_2(\text{Pyr swivel})$
1161	1154	$\nu_{52} \delta(\text{C}_\beta\text{H})$	363		$\delta(\text{C}'_2\text{C}_1\text{C}'_2)$, <i>t</i> Bu scis.
1066	1078/1069	$\nu_{44} \nu(\text{Pyr}/2)_{\text{as}}$	348		$\gamma_7 \gamma(\text{C}_\alpha\text{N}_m)$
1028	1028	CH ₃ wag	295		CH ₃ torsion
1007	1011	$\nu_{47} \nu(\text{Pyr breath})$	260		$\gamma_6 \gamma(\text{Pyr tilt})$
922	905	$\nu(\text{C}_1\text{C}_2)$	235		CH ₃ torsion
865		$\nu_{45} \nu(\text{C}_\beta'\text{C}_1)$	213		CH ₃ torsion
785	799	$\nu_{46} \delta(\text{Pyr def})_{\text{as}}$	115		$\gamma_9 \gamma(\text{Cu-N}_p)$
753	772	$\nu_{48} \delta(\text{Pyr def})_s$	55		<i>t</i> Bu torsion
583	596	$\delta(\text{C}_2\text{C}_1\text{C}'_2)$, <i>t</i> Bu umbr.	31		$\gamma_3 \gamma(\text{C}_\beta'\text{C}_1)$
530		$\nu_{49} \delta(\text{Pyr rot.})$			
437		$\nu_{50} \nu(\text{Cu-N}_p)$			
380		$\delta(\text{C}'_2\text{C}_1\text{C}'_2)$, <i>t</i> Bu scis.			
313		$\nu_{53}(\text{Pyr transl.})$			
281		CH ₃ torsion			
256		CH ₃ torsion			
225		$\delta(\text{C}_\beta'\text{C}_1\text{C}_2)$, <i>t</i> Bu wag			
97		$\delta(\text{C}_\beta\text{C}_\beta'\text{C}_1)$, <i>t</i> Bu rock			

^a with 6-31G(d) basis sets for C, N, H and TZVP for Cu. Scaling factor=0.97.

^b from IR spectra (KBr pellet).

^c Mode descriptions according to Refs.[19, 21].

the 1440–1650 cm^{-1} region due to the relatively large force constants. As is shown in Fig.4, the 514.5 nm excited spectrum of CuT(*t*Bu)TAP gives rise to four strong bands in this region, at 1569, 1519, 1469, and 1441 cm^{-1} , respectively. We consider that these bands correspond to the calculated bands at 1568, 1533, 1479, and 1445 cm^{-1} . Based on the B3LYP calculations, we assign the observed bands at 1569, 1519, 1469, and 1441 cm^{-1} to the ν_2 ($\text{C}_\beta\text{C}_\beta'$ stretching of A_g symmetry), ν_{10} (asymmetric $\text{C}_\alpha\text{N}_m$ stretching of B_g symmetry), ν_{19} (asymmetric $\text{C}_\alpha\text{N}_m$ stretching of A_g symmetry), and ν_{28} (symmetric $\text{C}_\alpha\text{N}_m$ stretching of B_g symmetry), respectively. Besides, DFT calculation predicted that ν_3 (the symmetric $\text{C}_\alpha\text{N}_m$ stretching, A_g symmetry) and ν_{11} ($\text{C}_\beta\text{C}_\beta'$ stretching, B_g symmetry) should also appear at 1464 and 1574 cm^{-1} . Experimentally, we

have not measured these two modes in the Raman spectrum, which may be attributed either to their weak intensities or to the band overlapping.

The pyrrole half-ring and quarter-ring stretching modes of CuT(*t*Bu)TAP are known to locate in the region 1000–1450 cm^{-1} . The strongest band in this region was observed at 1308 cm^{-1} , which can be readily correlated to the calculated band at 1302 cm^{-1} . It is assigned to ν_{12} , the symmetric pyrrole half ring stretching of B_g symmetry. Other bands in this region were observed at 1406, 1341, 1210, 1145, and 1085 cm^{-1} , corresponding to calculated bands at 1395, 1328, 1215, 1147, and 1088 cm^{-1} . We assigned them to the symmetric pyrrole half ring stretching of A_g symmetry (ν_4), pyrrole quarter ring stretching of B_g symmetry (ν_{29}), asymmetric pyrrole half ring stretching of A_g symmetry

TABLE III B3LYP-calculated and observed A_g mode frequencies (in cm^{-1}) of CuT(*t*Bu)TAP together with the observed frequencies of MT(*t*Bu)TAP (M=Co, Ni, and Zn).

Cu			Co	Ni	Zn
Cal. ^a	Obs. ^b	Assign. ^c	Obs. ^b	Obs. ^b	Obs. ^b
1568	1569	$\nu_2 \nu(C_\beta C_\beta')$	1576	1579	1561
1510		CH ₃ scis.			
1489		CH ₃ scis.			
1479	1469	$\nu_{19} \nu(C_\alpha N_m)_{as}$	1486	1495	1447
1474		CH ₃ scis.			
1464		$\nu_3 \nu(C_\alpha N_m)_s$			
1411		CH ₃ umbr.			
1395	1406	$\nu_4 \nu(\text{Pyr}/2)_s$		1409	1404
1381		CH ₃ umbr.			
1307		$\nu_{20} \nu(\text{Pyr}/4)$			
1244		$\nu_{26} \delta(C_\beta H)/\nu(C_\beta' C_1)$			
1215	1210	$\nu_{22} \nu(\text{Pyr}/2)_{as}$	1210	1211	1222
1186		$\nu_9 \delta(C_\beta H)$			
1066		$\nu_{23} \nu(C_\beta' C_1)/\delta(C_\beta H)$			
1020		$\nu_6 \nu(\text{Pyr breath})$			
1023		CH ₃ wag			
921		$\nu(C_1 C_2)$			
865		$\nu_5 \nu(C_\beta' C_1)$			
783	734	$\nu_{24} \delta(\text{Pyr def})_{as}$	732	754	765
704		$\nu_7 \delta(\text{Pyr def})_s$			
600	619	$\nu_{25} \delta(\text{Pyr rot})$	610		612
545		$\delta(C_2 C_1 C_2')$, <i>t</i> Bu umbr.			
433	454	$\nu_8 \nu(\text{M}-N_p)$	452	454	450
395	398	$\delta(C_2' C_1 C_2'')$, <i>t</i> Bu scis.	399		
299		$\delta(C_2' C_1 C_2'')$, <i>t</i> Bu scis.			
274		CH ₃ torsion			
227	(224)	$\delta(C_\beta' C_1 C_2)$			
145		$\delta(C_\beta C_\beta' C_1)$			

^a with 6-31G(d) basis sets for C, N, H; TZVP for Cu.

Scaling factor is 0.97.

^b Raman spectra from solid powder.

^c Mode descriptions according to Refs.[19, 21].

(ν_{22}), $C_\beta H$ in-plane bending of B_g symmetry (ν_{34}), and $C_\beta' C_1$ stretching of B_g symmetry (ν_{31}), respectively. For ν_{31} , DFT calculation indicates that the stretching of $C_\beta' C_1$ bonds is strongly coupled with the in-plane bending of $C_\beta' C_\beta H$ bond-angle, which may be attributed to the asymmetric substitution of *tert*-butyl group on the pyrrole rings. The Raman band near 1030 cm^{-1} in the 514.5 nm excited spectrum is rather broad (Fig.4(b)). According to the B3LYP calculation, it can be considered due to the overlap of the pyrrole breathing vibration of B_g symmetry (ν_{15} , calculated at 1020 cm^{-1}) and the asymmetric pyrrole half ring stretch of B_g symmetry (ν_{30} , calculated at 1034 cm^{-1}).

The Raman active bands due to pyrrole deformation,

TABLE IV B3LYP-calculated and observed B_g mode frequencies (in cm^{-1}) of CuT(*t*Bu)TAP together with the observed frequencies of MT(*t*Bu)TAP (M=Co, Ni, and Zn).

Cu			Co	Ni	Zn
Cal. ^a	Obs. ^b	Assign. ^c	Obs. ^b	Obs. ^b	Obs. ^b
1574		$\nu_{11} \nu(C_\beta C_\beta')$			
1533	1519	$\nu_{10} \nu(C_\alpha N_m)_{as}$	1517	1531	1507
1508		CH ₃ scis.			
1487		CH ₃ scis.			
1477		CH ₃ scis.			
1445	1441	$\nu_{28} \nu(C_\alpha N_m)_s$	1458	1472	1426
1410		CH ₃ umbr.			
1382		CH ₃ umbr.			
1328	1341	$\nu_{29} \nu(\text{Pyr}/4)$			
1302	1308	$\nu_{12} \nu(\text{Pyr}/2)_s$	1331	1332	1310
1252		$\nu_{14} \nu(C_\beta' C_1)/\delta(C_\beta H)$			
1212		$\nu(C_1 C_2)/\delta(C_2' C_1 C_2'')$			
1147	1145	$\nu_{34} \delta(C_\beta H)$	1148	1164	1143
1088	1085	$\nu_{31} \nu(C_\beta' C_1)/\delta(C_\beta H)$	1087	1083	1085
1034	(1030)	$\nu_{30} \nu(\text{Pyr}/2)_{as}$			
1020	1030	$\nu_{15} \nu(\text{Pyr breath})$	1044	1046	1027
922		$\nu(C_1 C_2)$			
881		$\nu_{17} \delta(C_\beta H)/\nu(C_\beta' C_1)$			
797		$\nu_{32} \delta(\text{Pyr def})_{as}$			
742	723	$\nu_{16} \delta(\text{Pyr def})_s$	725	726	723
612		$\nu_{33} \delta(\text{Pyr rot})$			
539	575	$\delta(C_2 C_1 C_2')$, <i>t</i> Bu umbr.	580	580	573
388		$\delta(C_2' C_1 C_2'')$, <i>t</i> Bu scis.			
361		$\delta(C_2' C_1 C_2'')$, <i>t</i> Bu scis.			
273		CH ₃ torsion			
262		$\delta(C_\beta' C_1 C_2)$			
221	224	$\nu_{35} \delta(\text{Pyr trans.})$	239	245	228
162		$\nu_{18} \nu(\text{M}-N_p)$			
88		$\delta(C_\beta C_\beta' C_1)$			

^a with 6-31G(d) basis sets for C, N, H; TZVP for Cu.

Scaling factor is 0.97.

^b Raman spectra from solid powder.

^c Mode descriptions according to Refs.[19, 21].

rotation and translation vibrational modes were calculated below 900 cm^{-1} . The strong band observed at 723 cm^{-1} and the shoulder band at 734 cm^{-1} are assigned to the pyrrole deformation vibrations ν_{16} (B_g symmetry) and ν_{24} (A_g symmetry), respectively. The observed weak band at 619 cm^{-1} is assigned to ν_{25} (pyrrole rotation, A_g symmetry), which was calculated at 600 cm^{-1} . The middle strong Raman band observed at 454 cm^{-1} is assigned to the Cu- N_p stretching of A_g symmetry (ν_8 mode), which was calculated at 433 cm^{-1} with a considerable intensity. The broad band of CuT(*t*Bu)TAP at 224 cm^{-1} is considered to be ν_{35} mode (pyrrole translation, B_g), which may overlap

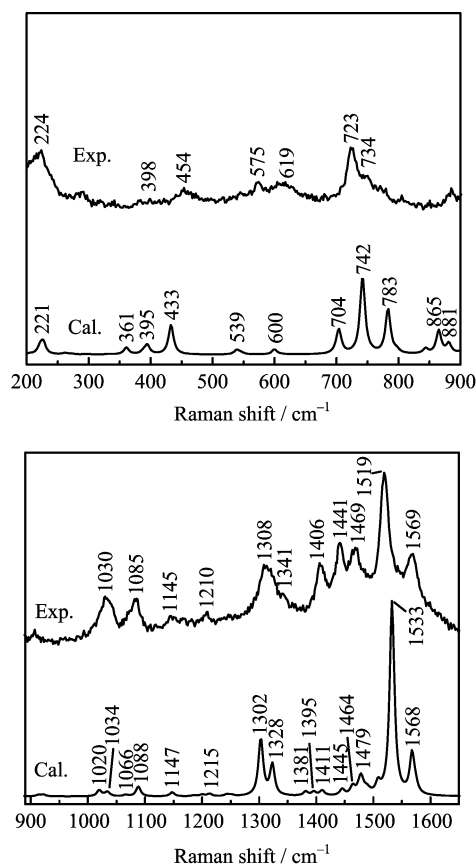


FIG. 4 Calculated and experimental Raman spectra (514.5 nm excitation) of CuT(*t*Bu)TAP.

with the $C_{\beta}'C_1C_2$ bending vibration (A_g symmetry).

2. Raman spectra of MT(*t*Bu)TAPs and their structural implications

The 514.5 nm excited Raman spectra of MT(*t*Bu)TAP (M=Cu, Ni, Co, Zn) are displayed in Fig.5. The observed Raman frequencies have been listed in Tables III and IV. As shown in Fig.5, different metal substitution generates systematic and regular changes in Raman spectra, which reflects the intrinsic connection between the molecular structures and the vibrational frequencies. For normal metalloporphyrins, empirical correlations have been found between the positions of Raman bands and the porphyrin core-size C_t-N_p (*i.e.*, the distance between the center of the porphyrin ring and the pyrrole nitrogen atom) [17, 18]. Especially, the Raman bands due to the stretching of the $C_{\beta}C_{\beta}$ and $C_{\alpha}C_m$ bonds have been found sensitive to the core-size change [17, 18].

For MT(*t*Bu)TAPs, DFT calculations predicted six such vibrations (*i.e.*, ν_2 , ν_3 , ν_{19} , ν_{10} , ν_{11} , and ν_{28}) to appear in the region 1440–1660 cm^{-1} . Experimentally, ν_2 , ν_{19} , ν_{10} , and ν_{28} were measured in the 514.5 nm excited Raman spectra, whereas ν_3 and ν_{11} were not

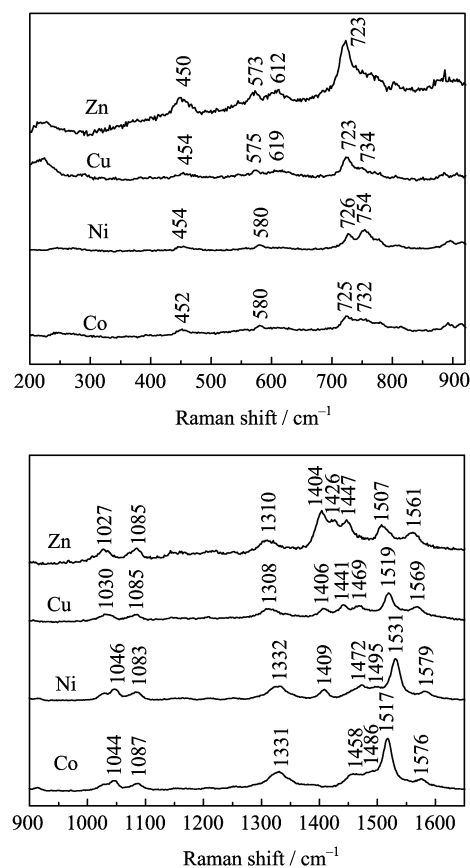


FIG. 5 Experimental 514.5 nm excited Raman spectra of MT(*t*Bu)TAP (M=Cu, Ni, Co, Zn).

observed due to their weak intensities. We have studied the frequency/core-size relationship of MT(*t*Bu)TAP by correlating the observed Raman frequencies with the calculated M– N_p distances. Figure 6 displays the relationships between the core-size (M– N_p distance) and the frequencies of ν_2 , ν_{10} , ν_{19} , and ν_{28} modes. It can be found the frequencies of ν_2 ($C_{\beta}C_{\beta}'$ stretching, A_g symmetry), ν_{19} (asymmetric $C_{\alpha}N_m$ stretching, A_g symmetry), and ν_{28} (symmetric $C_{\alpha}N_m$ stretching, B_g symmetry) change linearly with the core-sizes. The slope of the line reflects the relative sensitivity of a specific vibrational frequency to the core-size change. We found that with the decrease of core-size by 0.01 Å, the frequencies of ν_2 , ν_{19} , and ν_{28} increase by 2.29, 5.82, and 5.61 cm^{-1} , respectively. It is clear that the ν_{28} and ν_{19} modes are more sensitive with respect to the ring expansion in comparison with the ν_2 mode. This general trend is coincident with normal metalloporphyrins for which $C_{\alpha}C_m$ stretching vibrations have been found more sensitive to the core-size change in comparison with the $C_{\beta}C_{\beta}$ stretching vibrations [17, 18].

As shown in Fig.6, the core-size correlation for the ν_{10} mode is quite poor. The calculated Cartesian displacements indicate that, while ν_{10} is nominally assigned to the asymmetric $C_{\alpha}N_m$ stretching, it contains a signif-

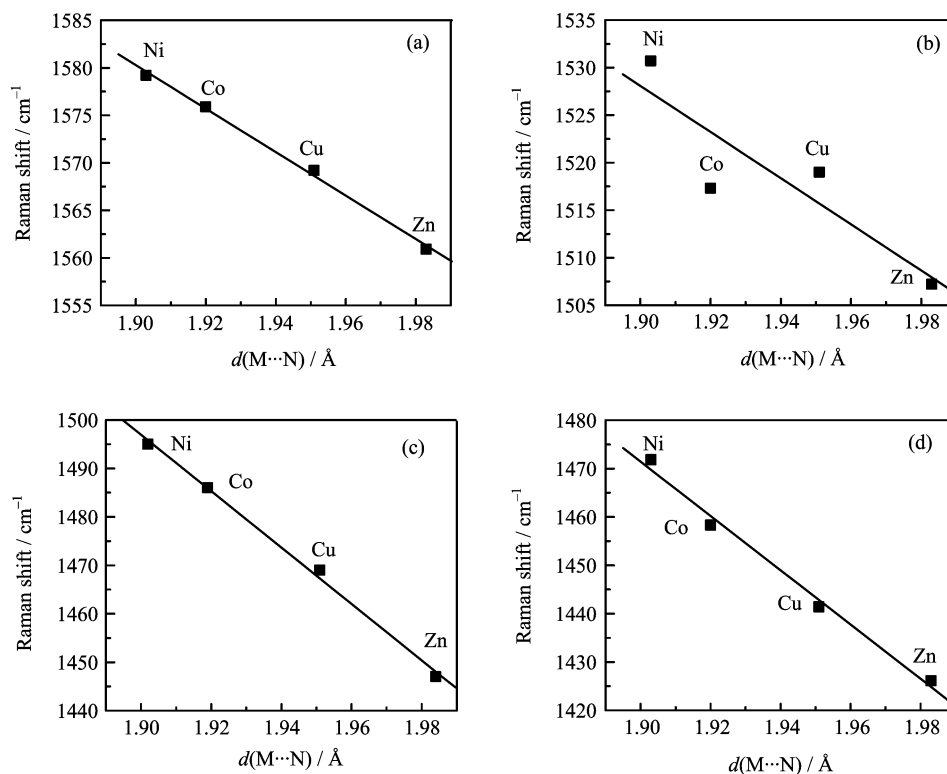


FIG. 6 Correlation between the Raman frequencies (for ν_2 (a), ν_{10} (b), ν_{19} (c), and ν_{28} (d) modes) and the calculated core-sizes of MT(*t*Bu)TAP (M=Co, Ni, Cu, Zn). Frequencies from solid spectra excited at 514.5 nm.

icant component of $C_\beta C_{\beta'}$ stretching. In addition, we found that the $C_1 C_{\beta'}$ stretching also contributes to the ν_{10} mode. This kind of vibrational coupling is partially attributable to the asymmetric substitution of the tert-butyl group on the pyrrole rings. We consider that the poor core-size/frequency correlation for the ν_{10} mode is probably due to the change of normal mode compositions for different MT(*t*Bu)TAP complexes.

IV. CONCLUSION

We have studied the ground-state structures of MT(*t*Bu)TAPs (M=Cu, Co, Ni, Zn) with density functional theory using B3LYP functional. The calculating results indicate that all the four compounds have planar TAP rings with C_{4h} symmetry. The measured IR spectra of MT(*t*Bu)TAPs were found basically in accordance with the calculations. The 514.5 nm Raman spectra of MT(*t*Bu)TAPs have been measured and the observed Raman bands were assigned based on the DFT calculations. The relationship between the Raman/IR frequencies and the structure of TAP ring was investigated. It was found that the frequencies of the $C_\beta C_{\beta'}$ stretch (A_g), asymmetric $C_\alpha N_m$ stretch (A_g), and symmetric $C_\alpha N_m$ stretch (B_g) modes increase linearly with the decrease of the core-size of TAP rings.

V. ACKNOWLEDGMENTS

This work is supported by the National Natural Science Foundation of China (No.20473078) and the Education Department of China (No.SRFDP 200803580022).

- [1] T. P. Forsyth, D. B. G. Williams, A. G. Montalban, C. L. Stern, A. G. M. Barrett, and B. M. Hoffman, *J. Org. Chem.* **63**, 331 (1998).
- [2] B. Cosimelli, G. Roncucci, D. Dei, L. Fantetti, F. Ferroni, M. Ricci, and D. Spinelli, *Tetrahedron* **59**, 10025 (2003).
- [3] P. Kubát and J. Mosinger, *J. Photochem. Photobiol. A* **96**, 93 (1996).
- [4] G. Li, S. K. Pandey, A. Graham, M. P. Dobhal, R. Mehta, Y. Chen, A. Gryshuk, K. Rittenhouse-Olson, A. Oseroff, and R. K. Pandey, *J. Org. Chem.* **69**, 158 (2004).
- [5] A. G. Montalban, W. Jarrell, E. Riguet, Q. J. McCubbin, M. E. Anderson, A. J. P. White, D. J. Williams, A. G. M. Barrett, and B. M. Hoffman, *J. Org. Chem.* **65**, 2472 (2000).
- [6] W. Freyer and S. Flatau, *Tetrahedron Lett.* **37**, 5083 (1996).
- [7] J. P. Fitzgerald, B. S. Haggerty, A. L. Rheingold, L. May, and G. A. Brewer, *Inorg. Chem.* **31**, 2006 (1992).

- [8] P. A. Stuzhin, M. Hamdush, and U. Ziener, *Inorg. Chim. Acta* **236**, 131 (1995).
- [9] Y. Ni, J. P. Fitzgerald, P. Carroll, and B. B. Wayland, *Inorg. Chem.* **33**, 2029 (1994).
- [10] N. Kobayashi, S. I. Nakajima, and T. Osa, *Inorg. Chim. Acta* **210**, 131 (1993).
- [11] N. Kobayashi and S. I. Nakajima, *Chem. Eur. J.* **10**, 6294 (2004).
- [12] Z. M. Chen, Y. Q. Wu, X. Zuo, and Y. L. Song, *Chin. J. Inorg. Chem.* **22**, 47 (2006).
- [13] Z. M. Chen, Y. Q. Wu, and X. Zuo, *Dyes and Pigments* **73**, 245 (2007).
- [14] W. Freyer, C. C. Neacsu, and M. B. Raschke, *J. Lumin.* **128**, 661 (2008).
- [15] D. Braun and A. Ceulemans, *J. Phys. Chem.* **99**, 11101 (1995).
- [16] L. Guo, D. E. Ellis, B. M. Hoffman, and Y. Ishikawa, *Inorg. Chem.* **35**, 5304 (1996).
- [17] W. A. Oertling, A. Salehi, Y. C. Chung, G. E. Leroi, C. K. Chang, and G. T. Babcock, *J. Phys. Chem.* **91**, 5887 (1987).
- [18] N. Parthasarathi, C. Hansen, S. Yamaguchi, and T. G. Spiro, *J. Am. Chem. Soc.* **109**, 3865 (1987).
- [19] X. Y. Li, R. S. Czernuszewicz, J. R. Kincaid, Y. O. Su, and T. G. Spiro, *J. Phys. Chem.* **94**, 31 (1990).
- [20] Z. Y. Li, T. T. Lu, T. J. He, F. C. Liu, and D. M. Chen, *Chin. J. Chem. Phys.* **22**, 346 (2009).
- [21] T. S. Rush III, P. M. Kozlowski, C. A. Piffat, R. Kumble, M. Z. Zgierski, and T. G. Spiro, *J. Phys. Chem. B* **104**, 5020 (2000).
- [22] L. C. Xu, Z. Y. Li, W. Tan, T. J. He, F. C. Liu, and D. M. Chen, *Spectrochim. Acta A* **62**, 850 (2005).
- [23] E. J. Baerend, G. Ricciardi, A. Rosa, and S. J. A van Gisbergen, *Coord. Chem. Rev.* **230**, 5 (2002).
- [24] X. Liu, E. K. L. Yeow, S. Velate, and R. P. Steer, *Phys. Chem. Chem. Phys.* **8**, 1298 (2006).
- [25] L. C. Xu, Z. Y. Li, T. J. He, F. C. Liu, and D. M. Chen, *Chem. Phys.* **305**, 165 (2004).
- [26] T. T. Lu, M. Xiang, H. L. Wang, T. J. He, and D. M. Chen, *J. Mol. Struct. Theochem.* **860**, 141 (2008).
- [27] A. D. Becke, *J. Chem. Phys.* **98**, 5648 (1993).
- [28] C. Lee, W. Yang, and R. G. Parr, *Phys. Rev. B* **37**, 785 (1988).
- [29] A. Schaefer, H. Horn, and R. Ahlrichs, *J. Chem. Phys.* **97**, 2571 (1992).
- [30] A. Schaefer, C. Huber, and R. Ahlrichs, *J. Chem. Phys.* **100**, 5829 (1994).
- [31] M. J. Frisch, G. W. Trucks, H. B. Schlegel, G. E. Scuseria, M. A. Robb, J. R. Cheeseman, V. G. Zakrzewski, J. A. Montgomery Jr., R. E. Stratmann, J. C. Burant, S. Dapprich, J. M. Millam, A. D. Daniels, K. N. Kudin, M. C. Strain, O. Farkas, J. Tomasi, V. Barone, M. Cossi, R. Cammi, B. Mennucci, C. Pomelli, C. Adamo, S. Clifford, J. Ochterski, G. A. Petersson, P. Y. Ayala, Q. Cui, K. Morokuma, D. K. Malick, A. D. Rabuck, K. Raghavachari, J. B. Foresman, J. Cioslowski, J. V. Ortiz, A. G. Baboul, B. B. Stefanov, G. Liu, A. Liashenko, P. Piskorz, I. Komaromi, R. Gomperts, R. L. Martin, D. J. Fox, T. Keith, M. A. Al-Laham, C. Y. Peng, A. Nanayakkara, C. Gonzalez, M. Challacombe, P. M. W. Gill, B. Johnson, W. Chen, M. W. Wong, J. L. Andres, C. Gonzalez, M. Head-Gordon, E. S. Replogle, and J. A. Pople, *Gaussian 03*, Pittsburgh, PA: Gaussian Inc. (2003).
- [32] Y. H. Zhang, W. Zhao, J. Wang, and P. Jiang, *Spectrochim. Acta A* **75**, 499 (2010).
- [33] Y. H. Zhang, W. Zhao, P. Jiang, L. J. Zhang, T. Zhang, and J. Wang, *Spectrochim. Acta A* **75**, 880 (2010).
- [34] R. E. Oakes and S. E. J. Bell, *J. Phys. Chem. A* **107**, 10953 (2003).
- [35] E. B. Wilson Jr., J. C. Decius, and P. C. Cross, *Molecular Vibrations*, New York: Dover Publications Inc. (1955).